Articles

Crystal Structure of Bovine Low Molecular Weight Phosphotyrosyl Phosphatase Complexed with the Transition State Analog Vanadate[†,‡]

Marie Zhang,[§] Ming Zhou,[§] Robert L. Van Etten,*[,§] and Cynthia V. Stauffacher*[,||]

Departments of Chemistry and Biological Sciences, Purdue University, West Lafayette, Indiana 47907

Received July 22, 1996; Revised Manuscript Received October 9, 1996[⊗]

ABSTRACT: The early transition metal oxoanions vanadate, molybdate, and tungstate are widely used inhibitors for phosphatase enzymes. These oxoanions could inhibit such enzymes by simply mimicking the tetrahedral geometry of phosphate ion. However, in some cases, the enzyme−inhibitor dissociation constants (K_i) for these oxoanions are much lower than that for phosphate. Such observations gave rise to the hypothesis that in some cases these transition metal oxoanions may inhibit phosphomonoesterases by forming complexes that resemble the trigonal bipyramidal geometry of the $S_N2(P)$ transition state. As a test of this, the crystal structures of a low molecular weight protein tyrosine phosphatase at pH 7.5 complexed with the inhibitors vanadate and molybdate were solved at 2.2 Å resolution and compared to a newly refined 1.9 Å structure of the enzyme. Geometric restraints on the oxoanions were relaxed during refinement in order to minimize model bias. Both inhibitors were bound at the active site, and the overall protein structures were left unchanged, although some small but significant side chain movements at the active site were observed. Vanadate ion formed a covalent linkage with the nucleophile Cys^{12} at the active site and exhibited a trigonal bipyramidal geometry. In contrast, simple tetrahedral geometry was observed for the weaker molybdate complex. These studies are consistent with the conclusion that vanadate inhibits tyrosine phosphatases by acting as a transition state analog. The structure of the vanadate complex may be expected to closely resemble the transition state for reactions catalyzed by protein tyrosine phosphatases.

Protein phosphorylation is one of the major signal transduction mechanisms for controlling and regulating intracellular processes. The extent of tyrosine phosphorylation reflects the carefully tuned balance between the action of protein tyrosine kinases (PTKs) and protein tyrosine phosphatases (PTPases).[1] On the basis of sequence homology and substrate specificity comparisons, PTPases can be categorized into several subfamilies including the high molecular weight PTPases (Charbonneau & Tonks, 1992; Zhang & Dixon, 1994), the low molecular weight PTPases (Zhang et al., 1995), and the dual specificity PTPases (Blenis, 1993). The high and low molecular weight PTPases share little sequence identity, with the exception of the universal PTPase sequence CXXXXXR(S/T) at the active site. Recently, the structures of several PTPases have been solved. It has been found that PTP1B (Barford et al., 1994) and *Yersinia* PTPase (Stuckey et al., 1994), which belong to the nonreceptor high molecular weight PTPase family, share a considerable amount of structural similarity. In contrast, the structure of bovine low M_r PTPase (BPTP) (Zhang, M., et al., 1994a; Su et al., 1994; Logan et al., 1994), a member of the low molecular weight PTPase family, has a fold distinct from these two and does not resemble the structure of high molecular weight PTPases. The structure of BPTP is typical of $\alpha\beta$ proteins, containing a central four-stand parallel β sheet with flanking α helices on both sides. The overall topology falls into the "Rossmann fold" category, with the active site of the molecule located at the C-terminal end of the β sheet (Zhang, M., et al., 1994a). The only structural similarity between the low and high M_r PTPases is at the active site, where the loop which contains the PTPase sequence motif and other critical residues occupy nearly identical positions (Zhang et al., 1995).

The catalytic mechanism of the low M_r PTPases has been extensively investigated. Biochemical evidence showed that the low M_r PTPases catalyze the dephosphorylation of phosphomonoesters by a two-step mechanism, in which each step of the reaction is accompanied by an inversion of configuration at the phosphorus atom (Saini et al., 1981). Each of these reaction steps can be regarded as proceeding through a trigonal bipyramidal transition state characteristic of an $S_N2(P)$ reaction. The first step is a phosphorylation in which the enzyme binds the phosphate monoester to form a Michaelis complex, followed by the rapid formation of a covalent phosphoenzyme intermediate (Davis et al., 1994b).

[†] This work was supported by USDHHS Research Grant GM 27003, by the Indiana Elks Foundation, and by a grant from the Lucille P. Markey Foundation for the expansion of Structural Biology in the Department of Biological Sciences.

[‡] The atomic coordinates of the BPTP complex with HEPES, vanadate, and molybdate have been deposited with the Brookhaven Protein Data Bank under the filenames 2PNT, 3PNT, and 4PNT, respectively.

* Authors to whom correspondence may be addressed.

[§] Department of Chemistry.

[||] Department of Biological Sciences.

[⊗] Abstract published in *Advance ACS Abstracts,* November 15, 1996.

[1] Abbreviations: PTPase, protein tyrosine phosphatase; BPTP, bovine low M_r protein tyrosine phosphatase.

S0006-2960(96)01804-1 CCC: $14.00

This step is assisted by the protonation of the leaving group oxygen by a general acid (Zhang & Van Etten, 1991). In the second step, which is normally the rate-limiting step, the phosphoenzyme intermediate is attacked by a water molecule, forming a noncovalent enzyme−phosphate complex. Finally, inorganic phosphate is released from the enzyme. Correlation of these biochemical data with the structure of BPTP revealed the location of the nucleophilic cysteine (Cys^{12}) and an arginine (Arg^{18}) residue implicated in the enzymatic reaction, as well as a histidine (His^{72}) that affects the structure of the active site but is not essential for catalysis (Davis et al., 1994a,b). The structure also revealed an aspartic acid (Asp^{129}) that could act as proton donor in the first step of the catalytic reaction. This role was confirmed by site-directed mutagenesis and kinetic studies (Zhang, Z., et al., 1994). Other residues including Ser^{19} and Asn^{15} provide critical hydrogen-bonding interactions that affect the pK_a of Cys^{12} and the geometry of the backbone portion of the phosphate-binding loop (Evans et al., 1996).

The PTPases can be inhibited by a variety of natural and synthetic compounds. The early transition metal oxoanions including vanadate, molybdate, and tungstate are potent inhibitors of phosphomonoesterases, including the low M_r PTPases (Van Etten et al., 1974; Waheed et al., 1988). It was suggested earlier that the transition metal oxoanions bind tightly to numerous phosphatases, not merely because they behave as inorganic phosphate analogs but because they may make covalent linkages with the protein, forming trigonal bipyramidal complexes, and thus act as transition state analogs (Van Etten et al., 1974). The early transition metal oxoanions differ fundamentally from phosphate and sulfate ions in the rate at which ligand exchange occurs at the central atom. Thus, oxygen exchange of the transition metal oxoanions occurs within seconds at around neutral pH, in contrast to months for the oxygens of the phosphate ion (Murmann, 1977). The facile nature of such ligand addition/elimination reactions, coupled with the relative promiscuity with which the early transition metal oxoanions undergo covalent bonding to oxygen, nitrogen, and sulfur ligands, means that strong chelation can occur with a variety of amino acid side chains, providing of course that these ligands possess (*or can adopt*) an appropriate spatial organization.

Vanadium has been recognized as an essential nutritional requirement in higher animals for nearly a decade, although its function remains uncertain (Macara, 1980; Nielson, 1995). Studies *in vitro* have shown that vanadium is capable of decreasing the rate of respiration and oxidative phosphorylation (DeMaster & Mitchell, 1973). As vanadate, it can inhibit a variety of kinases and phosphatases and can catalyze the nonenzymatic oxidation of many biological compounds, such as phospholipids and catechols. Vanadate and tungstate mimic the effects of insulin (Barbera et al., 1994), while vanadate, molybdate, and tungstate can act to stabilize glucocorticoid receptors (Modarress et al., 1994). Many of these effects involve binding of the oxoanions to enzymes or receptors with associated phosphatase activity, but little information is available on the structure of such protein complexes.

The geometry of interaction of the vanadate ion can be complex, depending on the nature and geometry of the ligands (Pope & Dale, 1968; Van Etten et al., 1974). In recent work, the coordination geometry in solution of low molecular weight vanadium(V) complexes, particularly with simple N and O ligands, has been carefully characterized by Crans and her colleagues [cf. Crans et al. (1993) and Crans and Shin (1994)]. Novel vanadium(V) complexes with deprotonated amide nitrogens have been described by Cornman et al. (1994). Structural details of some proteins complexed with oxoanions have been described. A tungstate ion complexed in the active site of the $Fe^{2+}Mn^{2+}$-metalloprotein phosphatase 1 was present as a tetrahedral ion (Egloff et al., 1995). Ultraviolet, NMR, and Raman spectroscopy have been used to study various sugar and phosphoglucomutase complexes involving vanadate (Ray et al., 1990, 1993). Detailed structural information is available for several vanadate complexes of ribonuclease A (Wlodawer et al., 1983; Borah et al., 1985; Veenstra & Lee, 1994) and ribonuclease T1 (Kostrewa et al., 1989). In the former enzyme, vanadate is present as a distorted trigonal bipyramid, while in the latter it is present as a tetrahedral anion. A trigonal bipyramidal arrangement of oxygen atoms has also been found for a vanadate−ADP complex of S1 myosin (Smith & Rayment, 1996). The structure of a vanadium-containing chloroperoxidase that was crystallized from solutions containing 2 M azide ion showed that the vanadate was present as a trigonal bipyramidal ion with histidine and azide as axial ligands (Messerschmidt & Wever, 1996). In contrast, there is much less information available concerning the structure of bound vanadate with sulfur-containing protein ligands. The relatively weak inhibition of glycerol- and glyceraldehyde-3-phosphate dehydrogenases by vanadate ion has been examined kinetically and spectroscopically, and it was concluded that inhibition does not involve a reduction by thiol to vanadium(IV), but detailed structural information was not accessible (Crans & Simone, 1991). In the present study, we describe the structures of BPTP complexed with the early transition metal oxoanions, vanadate and molybdate. Direct structural evidence is presented that, at pH 7.5, the nucleophilic cysteine (Cys^{12}) forms a covalent adduct with vanadate, though not with molybdate. The structure of this vanadate complex is expected to closely resemble the transition state of reactions catalyzed by PTPases.

MATERIALS AND METHODS

Sodium orthovanadate was from Acros Organics (Pittsburgh, PA). Sodium tungstate ($Na_2WO_4 \cdot 2H_2O$), sodium molybdate ($Na_2MoO_4 \cdot 2H_2O$), and sodium phosphate dibasic heptahydrate ($Na_2HPO_4 \cdot H_2O$) were from Mallinckrodt Chemical Works. HEPES [*N*-(2-hydroxyethyl)piperazine-*N*′-2-ethanesulfonic acid sodium salt] was from Sigma Chemical Co. and Research Organics, Inc. Diethylmalonic acid was from Aldrich Chemical Co.

Recombinant bovine heart low M_r PTPase was overexpressed and purified to homogeneity according to the procedures described earlier (Wo et al., 1992). During the analysis of electron density maps in the course of solving the structure of BPTP (Zhang, M., et al., 1994a), an unknown spherical density was observed at the active site. An inorganic phosphate assay (Wo et al., 1992) of the protein stock used in the crystallization trials showed that the protein sample (10 mg/mL) contained 2−5 mM inorganic phosphate, so this spherical density at the active site was modeled as a phosphate ion. In order to prepare additional protein samples without bound phosphate at the active site, a desalting procedure was used. First, using a 7 cm, G-25 size-exclusion column (PD10 column, Pharmacia), the protein was ex-

Table 1: Diffraction Data and Refinement Statistics of the BPTP Complexes

complex	HEPES	vanadate	molybdate
data processing statistics			
resolution (Å)	∞−1.9	∞−2.2	∞−2.2
crystal (*n*)	1	3	1
measurements (*n*)	71205	40054	22738
unique reflections (*n*)	12122	6371	5870
% complete	98.3	80.1	73.3
R_{sym}[a]	0.065	0.066	0.066
refinement statistics			
resolution (Å)	20.0−1.9	20.0−2.2	20.0−2.2
reflections (*n*)	11869	6260	5798
R-factor[b] (%)	17.9	17.3	15.9
RMS bond lengths (Å)	0.010	0.010	0.010
RMS bond angles (deg)	2.34	2.32	2.45
torsion angle (deg)	14.2	14.1	14.2
av *B*-factor for complexed atoms (Å^2)	39.4	39.4	36.9

[a] $R_{sym} = \sum|(I_i - \langle I_i\rangle)|/\sum I_i$, where $\langle I_i\rangle$ is the average of I_i over all symmetry equivalents. [b] *R*-factor $= \sum|F_o - F_c|/\sum F_o$, where F_o and F_c are the observed and calculated structure factors.

changed from the purification buffer into a pH 5 buffer containing only 100 mM NaOAc. Each fraction was analyzed for inorganic phosphate content, and only protein fractions containing no detectable inorganic phosphate (i.e., $\leq$20 μM) were pooled. The concentrated protein was then passed through another PD10 column equilibrated with distilled water, producing the protein samples that were used for the crystallization trials.

The BPTP crystals were grown in 20% polyethylene glycol (PEG_{4k}), 10% 2-propanol in 100 mM HEPES buffer at pH 7.5 from protein at 10 mg/mL concentration prepared as described above. These crystals grew in a fashion similar to those prepared earlier using protein samples that contained inorganic phosphate (Zhang, M., et al., 1994b). Crystals complexed with vanadate and molybdate were prepared by transferring native crystals into crystallization buffer that contained vanadate or molybdate. Native crystals were soaked in either 0.5 mM Na_2VO_4 solution or 1 mM Na_2MoO_4 solution for 1 day prior to X-ray data collection. The native crystals were also soaked in 0.5−5 mM Na_2WO_4 solutions for various lengths of time from 1 to 5 days. The crystals of the complexes were isomorphous with the native crystals, with space group *C*2 and unit cell parameters a = 95.3 Å, b = 43.3 Å, c = 41.2 Å, and β = 113.4°.

X-ray data for the complexes were collected at 2.2 Å resolution on an image plate detector (R-Axis II; Molecular Structure Corp.) mounted on a Rigaku RU200 rotating anode X-ray generator operating at 50 kV and 100 mA. A native data set was also collected at 1.9 Å for the BPTP crystals that did not contain phosphate ion. The reflections were measured with 1.0° oscillation per frame and a 10 cm crystal to detector distance. Diffraction data were indexed and integrated by DENZO (Otwinowski, 1993), and then were merged and scaled by SCALEPACK (Otwinowski, 1993). The crystals complexed with vanadate and molybdate ions were far more sensitive to radiation damage, compared to the native crystal, limiting the resolution of the data collection to 2.2 Å. Data collection statistics for the native form and the complex data sets are summarized in Table 1.

Electron density maps ($2F_o - F_c$ and $F_o - F_c$) were calculated using phases from the refined model of native BPTP. Inspection of the electron density maps and model building was done with the graphics program O (Jones et al., 1991). The models of the (phosphate-free) native crystal with the HEPES molecule, and of the complexes with vanadate or molybdate, were refined using TNT (Tronrud et al., 1987) for positional and temperature factor refinement. The *R*-factors for data between 20 and 2.2 Å for the vanadate and molybdate complexes are 17.3% and 15.9%, respectively. The final models of the complexes possess good overall stereochemistry with root-mean-square (RMS) deviation of bond length and angles of 0.010 Å and 2.32° for the vanadate and 0.010 Å and 2.45° for the molybdate complexes. There were no outliers in the Ramachandran plots (Ramachandran & Sasisekharan, 1968) for either the vanadate or molybdate complexes.

Inhibition Constant K_i Measurements. Measurements of the dissociation constants (K_i) of the enzyme−inhibitor complexes were made at 37 °C. At pH 5.0, all K_i measurements were performed at an ionic strength of 0.15 M in 100 mM sodium acetate buffer solution. Six to eight substrate (pNPP) concentrations (0.15−1 mM) were used. At each substrate concentration, six to eight inhibitor concentrations were used for initial velocity measurements. During each initial velocity measurement, specific amounts of substrate stock solution (2−3 mM), inhibitor stock solution (0.01−2 mM), and buffer solution were mixed together. The final volume was 500 μL. At pH 7.5, all K_i measurements were performed at an ionic strength of 0.15 M in 25 mM DEM buffer solution. Six to eight substrate (pNPP) concentrations (3−20 mM) were used. At each substrate concentration, six to eight inhibitor concentrations were used for initial velocity measurements. During each initial velocity measurement, specific amounts of substrate stock solution (100 mM), inhibitor stock solution (0.01−2 mM), and buffer solution were mixed together. The final volume was 500 μL, and the final ionic strength was adjusted to 0.15 M with NaCl. These solutions were incubated for 5 min, and then 20 μL of BPTP solution was added. The reaction was allowed to proceed for 4 min and was stopped by addition of 500 μL of 1 N NaOH. The absorbance of the solution at 405 nm was measured using a Beckman DU-68 spectrophotometer. The initial velocities were calculated from the equation V_0 (unit/mg) $= 1.96A_{405}/((18.0 \times 4)/[E])$, where 1.96 is a dilution factor (the reaction solution was diluted by adding 500 μL of 1 N NaOH stop solution), 18.0 is the extinction coefficient in units of mM^{-1} cm^{-1}, 4 is the reaction time in minutes, and [E] is the enzyme concentration of the reaction in units of mg/mL. Measurements of V_0 were done with a series of inhibitor concentrations at each substrate concentration.

Data Processing. For each distinct substrate (pNPP) concentration, a plot of 1/initial velocity V_0 vs [I] was constructed by using a least squares linear fitting program in Quattro Pro 5.0 for Windows (Borland). This gave a family of straight lines intersecting in the second quadrant (cf. Figure 1). The absolute value of the projection of this intersection to the [I] axis is K_i. For all of the inhibitors described here, at both pH values, only competitive inhibition was observed.

RESULTS

Structure of the Native Protein without Inorganic Phosphate. The initial structure determination of BPTP was of

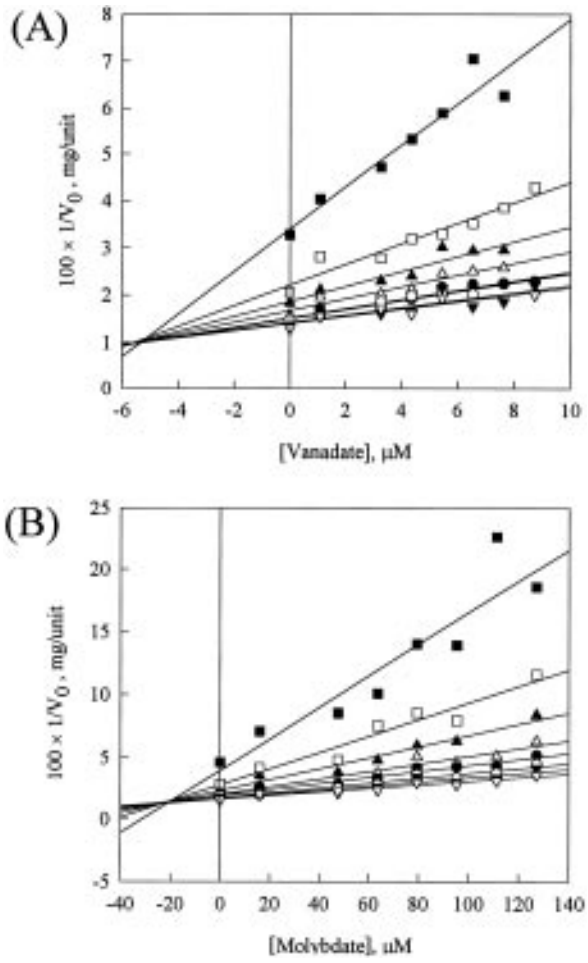

FIGURE 1: Competitive inhibition measurements. (A) Dixon plot (1/initial velocity V_0 versus inhibitor concentration) for the inhibition of BPTP by sodium vanadate. Measurements were made in 100 mM sodium acetate, I = 150 mM, at pH 5.0. The pNPP concentrations were (■) 0.13 mM, (□) 0.27 mM, (▲) 0.40 mM, (△) 0.54 mM, (●) 0.67 mM, (○) 0.80 mM, (▼) 0.94 mM, and (▽) 1.10 mM. (B) Dixon plot for the inhibition of BPTP by sodium molybdate. All measurements were made in 100 mM sodium acetate, I = 150 mM, at pH 5.0. The pNPP concentrations were (■) 0.10 mM, (□) 0.20 mM, (▲) 0.30 mM, (△) 0.40 mM, (●) 0.51 mM, (○) 0.61 mM, (▼) 0.71 mM, and (▽) 0.81 mM.

a form containing phosphate bound at the active site. During the refinement of this structure, an island of density with an irregular shape next to the phosphate density persisted in the $2F_o - F_c$ maps. Modeling a water molecule or another phosphate molecule into this density failed to fully explain the density. Another possibility was suggested by the fact that the protein was crystallized in HEPES buffer. Since sulfonic acid derivatives could potentially act as inhibitors, it was hypothesized that the unknown density at the active site could be that of the ring portion of a HEPES molecule present at partial occupancy. Consistent with this possibility, the determination of the inhibition constant for HEPES showed that it has a K_i comparable to that of phosphate ion (Table 2).

In order to do comparative studies of the native enzyme and the oxoanion complexes, crystals were produced of BPTP protein that had been desalted extensively to remove inorganic phosphate. It was anticipated that if the HEPES in the crystallization buffer did bind at the active site, then in the absence of inorganic phosphate the HEPES would be present at full occupancy and would appear in the maps

Table 2: Dissociation Constants (K_i) of BPTP−Inhibitor Complexes at pH 5.0 and 7.5[a]

	K_i (M)	
inhibitor	pH 5.0	pH 7.5
vanadate[b]	$5.4 \pm 0.8 \times 10^{-6}$	$1.0 \pm 0.6 \times 10^{-6}$
molybdate	$2.0 \pm 0.7 \times 10^{-5}$	$1.4 \pm 0.4 \times 10^{-3}$
tungstate	$5.0 \pm 1.3 \times 10^{-4}$	$3.3 \pm 0.6 \times 10^{-3}$
phosphate	$2.2 \pm 0.4 \times 10^{-3}$	$6.2 \pm 1.0 \times 10^{-3}$
HEPES	$5.3 \pm 0.8 \times 10^{-3}$	$1.8 \pm 0.8 \times 10^{-3}$

[a] In each case, competitive inhibition was observed. [b] Very weak complex formation has been observed between vanadate and acetic acid (Tracey et al., 1990), so acetic acid in the pH 5 measurement competes (weakly) with the enzyme for vanadate. Consequently, the actual K_i value at pH 5 may be somewhat closer to the pH 7.5 value as measured in the present experiments.

strongly. An initial $F_o - F_c$ difference electron density map was calculated from the observed phosphate-free BPTP native data with F_c's generated from only the protein coordinates, as determined from the previous BPTP structure containing inorganic phosphate. This map showed density at the active site which incorporated not only a spherical density at the position of the phosphate in the previously reported structure but also a directly connected, flattened density, consistent with a bound HEPES molecule. In order to accurately model the bound HEPES, the crystal structure of HEPES itself was solved by direct methods (P. Fanwick, and R. L. Van Etten, unpublished results). The resulting HEPES structure was readily modeled into the extended density at the active site, positioned such that the sulfonate group of HEPES occupied the same position as the inorganic phosphate. Thus, after removal of inorganic phosphate from protein solutions used for crystallization, a well-defined HEPES density appeared in both $F_o - F_c$ and $2F_o - F_c$ maps. Refinement of this BPTP−HEPES complex showed that the protein structure (Figure 2) is identical with the previously described BPTP−phosphate structure (Zhang, M., et al., 1994a, 1995). Numerous unsuccessful attempts were made to obtain crystals of BPTP without either the sulfonic acid derivative or inorganic oxoanions present at the active site. The difficulty of obtaining such a ligand-free enzyme may indicate that an ordering occurs in the structure upon substrate or inhibitor binding which facilitates crystal growth.

Structures of the Complexes of BPTP with Vanadate and Molybdate. The overall structures of the native enzyme and of the complexes of BPTP with the phosphatase inhibitors, vanadate and molybdate, are very similar. The RMS deviation of the Cα atoms of residues 5−157 is 0.216 Å between the phosphate-free native protein and the vanadate complex and 0.150 Å between this native protein and the molybdate complex.

The initial $F_o - F_c$ electron density maps for the complexes of BPTP with vanadate and molybdate (Figure 3) showed only a single strong spherical electron density at the active site (maximum at 10 times the standard deviation of the electron density map for vanadate and molybdate), indicating that the oxoanions had indeed replaced HEPES at the active site. No additional vanadate or molybdate binding sites were observed. The spherical electron density clearly showed that the species bound at the active site was a monooxoanion, despite the tendency of these early transition metal oxoanions to form polyanions. Similar soaking experiments at various conditions with tungstate ion were

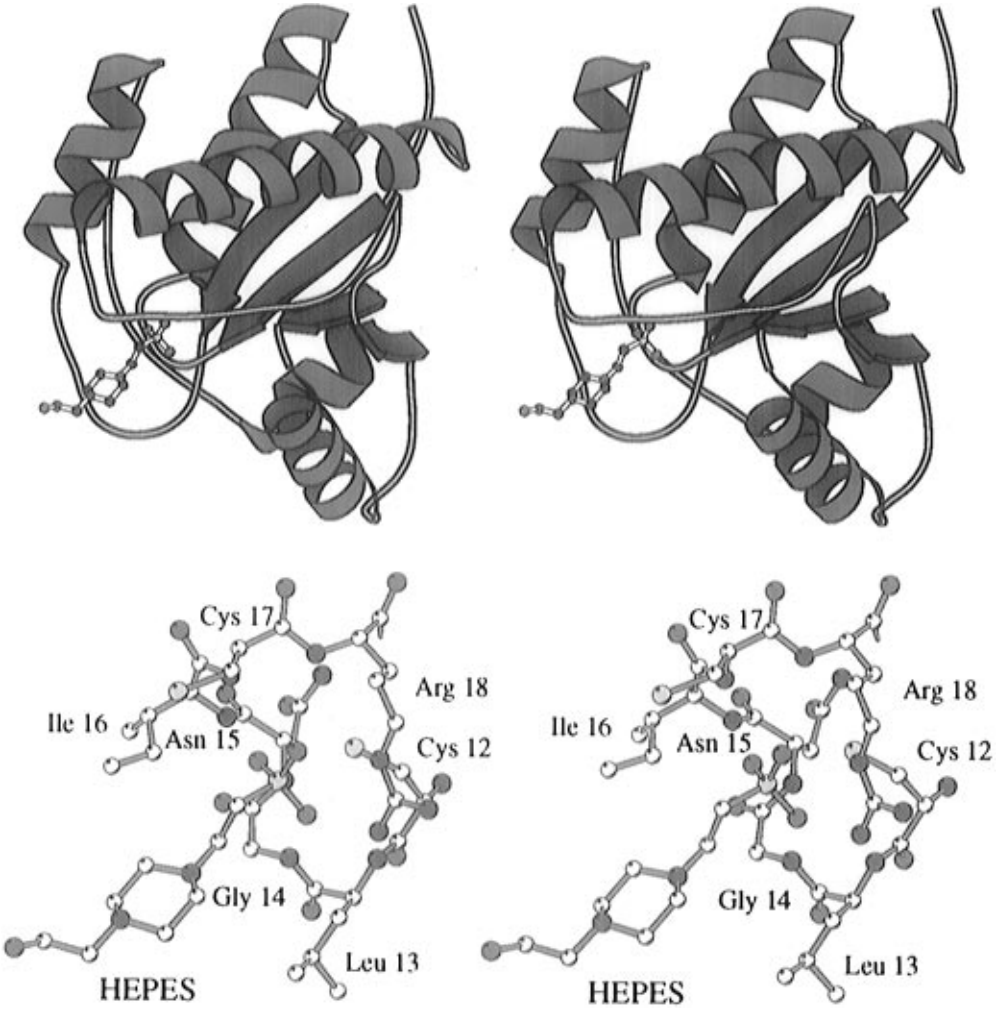

FIGURE 2: Native BPTP crystal structure with a HEPES buffer molecule bound at the active site. (A, top) Ribbon diagram of the BPTP structure. The HEPES molecule is illustrated as a ball and stick model with the sulfonate group sitting inside the active site. (B, bottom) Stereo illustration of the HEPES molecule bound in the active site loop (residues 12−18, CLGNICR). The sulfonate group of the HEPES molecule is situated in the same position as a phosphate group in the original BPTP structure (Brookhaven Protein Data Bank file 1PNT). The sulfonate group sits at the center of the active site loop, hydrogen bonding with the backbone amide hydrogens. Cys^{12}, the catalytic nucleophile, sits behind and in the center of the loop. Arg^{18}, in the foreground, curls around the sulfonate group, interacting with the oxygens through its NH's. The figure was generated by the program Molscript (Kraulis, 1991).

also performed. However, the $F_o - F_c$ electron density maps showed that tungstate at lower concentration was not bound to the protein, while at higher concentrations it polymerized to form a polyanion that was located at the crystallographic 2-fold, far from the active site.

The spherical electron density at the active site in the molybdate complex was virtually superimposable with the sulfonate density of the HEPES molecule in the native protein and with the phosphate ion in the original structure. In contrast, the electron density in the vanadate complex was at least 1 Å closer to the nucleophile Cys^{12} than were the densities for the molybdate complex or the HEPES sulfonate in the native protein (Figure 3). In addition to this closer position, a continuous electron density was observed in the $2F_o - F_c$ map between the side chain of Cys^{12} and the vanadium atom, when the map was contoured at a 1σ level (Figure 4). This electron density was located too close to Cys^{12} to be modeled as a tetrahedral vanadate ion. In addition, the electron density in the vanadate complex was not spherical, as it was in the case of the molybdate complex, but was instead flattened along the axis perpendicular to the Cys^{12} side chain. Consequently, when a trigonal bipyramidal geometry was modeled for vanadate ion, with Cys^{12} as an axial ligand, the structure fit very well into the density.

The BPTP structure complexed with vanadate ion was refined using the TNT refinement package. In order to avoid any model bias for the trigonal bipyramidal geometry suggested by the electron density map, a tetrahedral vanadate was first used in the refinement, but with loose constraints on the bond lengths (10 Å) and bond angles (20°) for the vanadate geometry. After 40 cycles of positional and individual *B*-factor refinement, the model showed that three of the four oxygens on the vanadate ion became nearly coplanar with the vanadium atom. Forty more cycles of refinement were done with increasingly tighter constraints of vanadate geometry on the previously refined model. In the final round of refinement, the three oxygen atoms and the vanadium were fixed in the same plane. A tetrahedral molybdate ion was modeled at the active site for the molybdate complex and refined with the protein. A refinement protocol similar to that employed for vanadate indicated that the molybdate ion was tetrahedral and situated at a position identical to that of the phosphate ion. In the first 40 cycles of refinement no substantial changes in the tetrahedral geometry of the molybdate were observed. That geometry was maintained through 40 more cycles of increas-

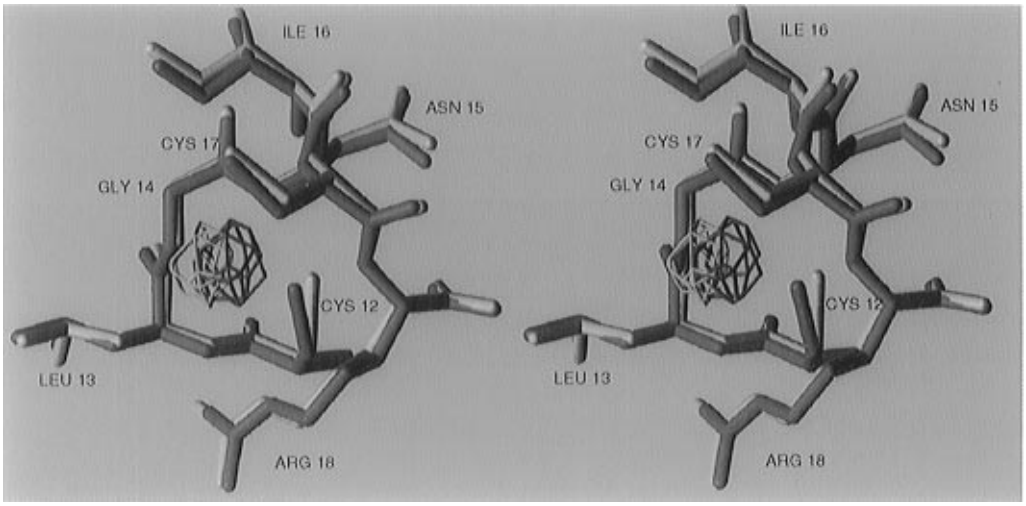

FIGURE 3: Initial $F_o - F_c$ electron density maps for the vanadate and molydate complexes of BPTP. Illustrated are active site residues of the complexes with vanadate (red) and molybdate (yellow), together with the generally spherical $F_o - F_c$ electron density for the oxoanions at the active site. The electron density maps are contoured at a 10σ level above background. The maximum density for the vanadate (green) is substantially closer to Cys^{12} than is the density for molybdate (blue). Cys^{12} moved 0.75 Å closer to the vanadium atom in the complex. A slight contraction in the active site loop and a shift in Arg^{18} can also be observed on binding of vanadate. This figure was generated by the program Molview (Smith, 1995).

ing constraints and fixed in the final round of refinement.

Cysteine Sulfur−Metal Distances in the Complexes. After refinement, the distances between the vanadium or molybdenum atom and the sulfur atom of the nucleophile Cys^{12} were 2.16 and 3.48 Å, respectively (Table 3). The short bond length of 2.16 Å strongly indicates the presence of a covalent bond to the cysteine sulfur in the vanadate complex, while the longer distance of 3.48 Å in the molybdate complex suggests hydrogen-bonding or noncovalent interactions. For comparison, a selection from the Cambridge Structural Database (Allen & Kennard, 1993) of 55 compounds containing apparently unstrained vanadium(V)−thiolate bonds showed a mean V−S bond distance of 2.39 ± 0.07 Å, while 378 compounds with Mo−S bonds showed a mean distance of 2.41 ± 0.09 Å.

Interactions of the Equatorial Oxygens of the Trigonal Bipyramid with the Phosphate-Binding Loop. The equatorial oxygens of the vanadate trigonal bipyramid exhibit strong hydrogen-bonding interactions with the backbone NH's and Arg^{18} side chain NH's (Table 4). When the O−N distances for the nine hydrogen-bonding interactions between the protein and the vanadate equatorial oxygens are compared with the O−N distances involving either sulfonate or phosphate oxygens, it is found that eight of the nine are shorter and thus apparently more favorable in the vanadate trigonal bipyramid. The average reduction in distance may be estimated as 0.12−0.18 Å. This is consistent with the interpretation that the transition state is differentially stabilized by hydrogen bonding, relative to the ground state or product phosphate complexes.

Movement of the Active Site Residues in the Enzyme−Vanadate Complex. The final model of the BPTP−vanadate complex demonstrated that the vanadate ion was bound to the BPTP protein in a trigonal bipyramidal geometry with Cys^{12} as a fifth axial ligand. Although the overall structure of the protein at the active site was not altered significantly, a few experimentally significant differences could be observed. The side chain of Cys^{12} moved 0.75 Å, with the sulfur rotating directly opposite the other axial oxygen ligand, in a position consistent with proper covalent binding to the vanadium atom. In addition, the entire active site loop appears to contract slightly, shifting the position of the side chain of the essential Arg^{18} toward the oxoanion (Figure 3).

DISCUSSION

Vanadium in solution has a complex chemistry, including multiple oxidation states, hydrolysis reactions, and polymerization equilibria. At physiological pH and above, vanadium exists in aqueous solution as a tetrahedral vanadate ion (HVO_4^{2-}) and tends to aggregate into polynuclear complexes at even moderate vanadate ion concentrations. Vanadate ions can also readily form chelates with a variety of groups including oxygen, nitrogen, and sulfur ligands. These chelates can form tetrahedral, octahedral, trigonal bipyramidal, and even square pyramidal complexes with varying metal−ligand bond distances (Pope & Dale, 1968; Van Etten et al., 1974).

The hypothesis that vanadate may inhibit enzymes by mimicking a transition state geometry was first proposed to explain the strong inhibition of ribonuclease by vanadate complexes of uridine (Lindquist et al., 1973). Subsequently, the possibility that the early transition metal oxoanions could act as transition state analogs was also proposed to explain the strong inhibition of phosphomonoesterases such as human lysosomal and prostatic acid phosphatases (Van Etten et al., 1974). Only recently has structural data been obtained in support of the latter proposal. Recently, Lindqvist et al., as part of their important studies on rat prostate acid phosphatase, concluded that, in complexes of that enzyme with vanadate and molybdate, the transition metal oxoanions appeared to exist in a geometry consistent with their action as transition state analogs (Lindqvist et al., 1994). In the case of that enzyme, the axial ligand in the trigonal bipyramidal transition metal oxoanion complex is histidine, instead of a cysteine as in BPTP. The bond distance measured between N and V atoms in that structure is 2.0 Å, which is slightly shorter than the S−V bond (2.16 Å) observed in the BPTP complex and substantially shorter than the histidine nitrogen−vanadate distance (2.25 Å) in a chloroperoxidase (Messerschmidt & Wever, 1996). How-

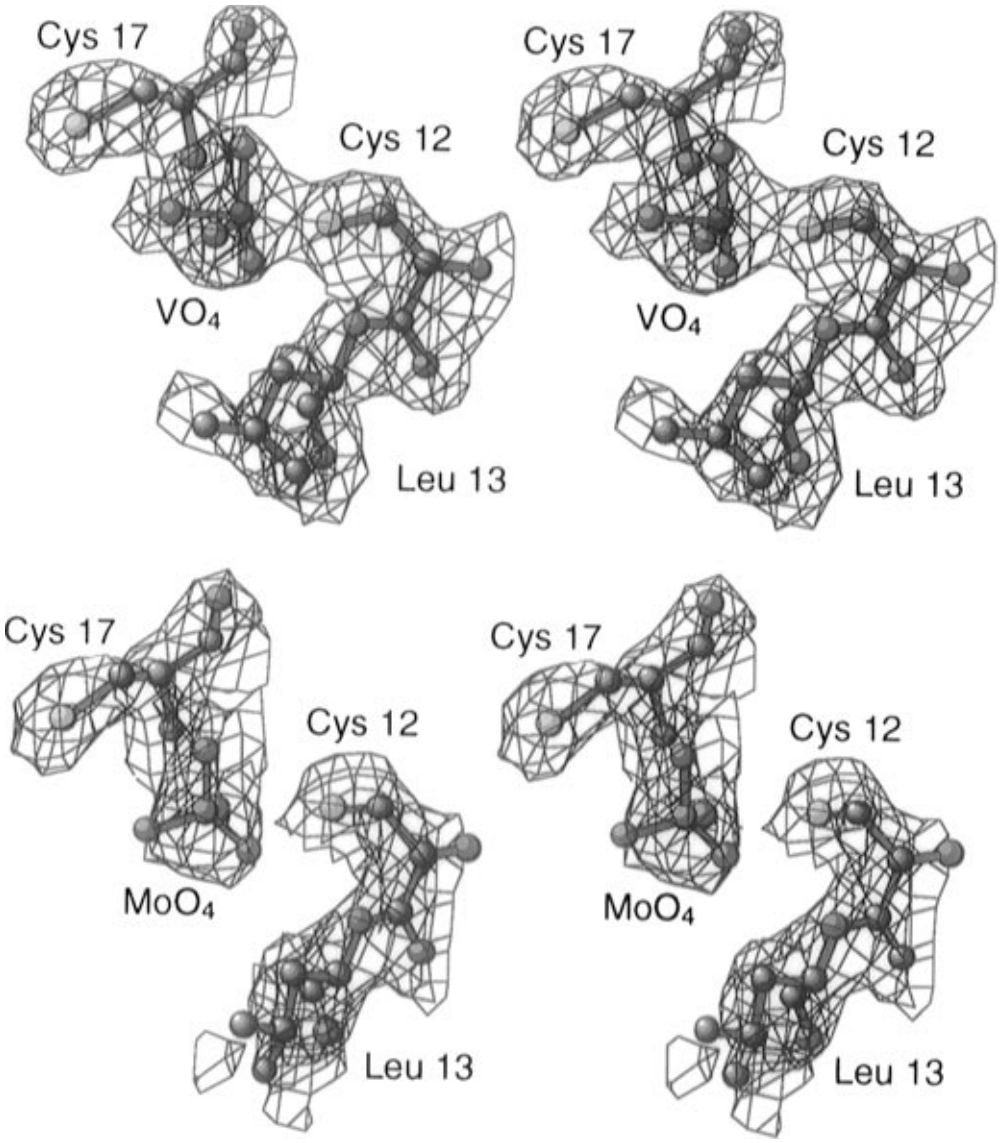

FIGURE 4: Initial $2F_o - F_c$ maps before refinement of the vanadate (top) and molybdate (bottom) complexes of BPTP. A continuous electron density between the side chain of Cys^{12} and the vanadium atom was observed for the vanadate complex but not for the molybdate complex. The map is contoured at a 1σ level. Superimposed on these initial maps are the final refined models of the two oxoanion complexes.

Table 3: Refined Bond Lengths and Bond Angles Involving Vanadium and Molydenum in the Respective Complexes with BPTP

atoms	bond distance (Å)	atoms	bond angles (deg)
V−O1	1.72 (axial oxygen)	O2−V−O1	82.91
V−O2	1.60	O1−V−O3	90.55
V−O3	1.62	O1−V−O4	85.53
V−O4	1.62	O2−V−O3	120.61
V−S1	2.16	O3−V−O4	118.20
		O2−V−O4	120.13
Mo−O1	1.73	O1−V−S1	173.70
Mo−O2	1.71	O2−V−S1	102.05
Mo−O3	1.73	O3−V−S1	83.58
Mo−O4	1.72	O4−V−S1	95.18
Mo−S1	3.48 (no bond)		
		O1−Mo−O2	112.50
		O1−Mo−O3	112.58
		O1−Mo−O4	101.42
		O2−Mo−O3	106.81
		O3−Mo−O4	117.04
		O2−Mo−O4	106.45

Table 4: Ligand Oxygen−Protein Nitrogen O−N Distances in BPTP Complexes

bond	HEPES sulfonate	PO_4	MoO_4	VO_4
O−N13	3.18	3.24	3.04	3.10
O−N14	2.99	2.88	2.95	2.83
O−N18 (sc)	2.93	2.92	2.87	3.26
O−N15	3.42	3.36	3.18	3.24
O−N16	3.03	2.87	2.69	2.55
O−N17	2.82	2.73	2.71	2.48
O−N18	3.25	3.30	3.09	2.80
O−N18 (sc)	2.87	2.79	2.89	2.76
O−N18 (sc)	3.61	3.40	3.71	3.38

ever, the resolution of the rat prostate phosphatase structure (3.0 Å) was substantially lower than these other two structures, so the differences in bond distance may not be significant. For comparison, in a higher resolution (1.9 Å) structure, the axial bond lengths to oxygen atoms in the myosin S1 complex of vanadate−ADP were 2.1 and 2.3 Å (Smith & Rayment, 1996).

In the structures of the rat prostate acid phosphatase complexes, both vanadate and molybdate reportedly exhibit a trigonal bipyramidal geometry. In contrast, in the present BPTP complexes, vanadate but not molybdate exhibited such a geometry. Differences in pH appear to be important. The structures of the complexes of rat prostate acid phosphatase

with vanadate and molybdate were determined at pH 5.4. At pH 5.0, vanadate and molybdate have similar K_i values (2.0×10^{-7} and 3.6×10^{-8} M, respectively) toward a homologous human acid phosphatase (Van Etten et al., 1974). In turn, this correlates very well with their similar mode of inhibition involving action as transition state analogs. However, the crystal structures of BPTP complexed with vanadate and molybdate were solved at pH 7.5. Although vanadate and molybdate have similar K_i values toward BPTP at pH 5.0 (Table 2), this is not true around neutral pH. At pH 7.5, the dissociation constant for the vanadate complex of BPTP is 3 orders of magnitude lower than that for the molybdate complex (1.0×10^{-6} and 1.4×10^{-3} M, respectively). The crystal structures of the BPTP transition metal oxoanion complexes correlate well with these enzyme inhibition data. For BPTP, the K_i value of molybdate at pH 7.5 is similar to that for phosphate (1.4 and 6.2 mM, respectively). This is consistent with the interpretation that the mechanism of inhibition by molybdate at neutral pH involves a simple mimicry of the phosphate geometry. The K_i data further suggest the possibility that, at pH 5.0, molybdate, as well as vanadate, may be expected to inhibit BPTP by acting as a transition state analog. The chemical basis for the pH-dependent mode of inhibition of BPTP by molybdate is not apparent.

Although the overall protein structures for the vanadate and molybdate complexes are nearly identical to the native structure, several significant differences can be seen at the active site. The movement of the nucleophile Cys^{12} sulfur into the position of an axial ligand for the vanadate is as expected. Covalent bond formation rather than just rapidly reversible association is consistent with earlier ^1H NMR data showing the appearance of two distinct resonances of the $C^{\epsilon 1}$ proton of His^{72} (which is adjacent to the active site) in the course of a titration of a homologous human enzyme with vanadate ion [see Figure 7 in Zhou et al. (1993)]. Because the vanadate ion bound at the active site is now in a trigonal bipyramidal form, the positions of the four oxygens on the vanadate ion are different from those on the tetrahedral phosphate. The side chain of the essential arginine (Arg^{18}), which contributes critical parts of the phosphate binding loop at the active site, moves correspondingly by 0.80 Å in order to ensure proper interactions of the terminal nitrogens with two of the three coplanar oxygens of the vanadate trigonal bipyramid. This leads us to suggest that Arg^{18} may have an unexpectedly critical role in the enzymatic reaction as it appears to participate actively in the stabilization of the transition state intermediate.

The analysis of the metal oxoanion−enzyme complexes presented here provides a structural basis to which some of the more intimate chemical details of the mechanism of enzymatic phosphomonoester hydrolysis can be related. Many phosphomonoesterases, including the protein tyrosine phosphatases PTP1B and cdc 25, have also been shown to be strongly inhibited by vanadate ion. Preliminary structural evidence described in Denu et al. (1996) suggests that a trigonal bipyramidal complex is formed with *Yersinia* PTPase. Despite the lack of sequence identity, all the PTPases found so far share very similar chemical mechanisms. In the known structures of PTPases, it can also be seen that, despite overall different folds, the structures of the active sites are virtually identical. Therefore, it is likely that vanadate inhibits PTPases by virtue of its action as a transition state analog throughout the entire PTPase family in the fashion revealed by these BPTP oxoanion complex structures.

ACKNOWLEDGMENT

The authors thank Dr. Phillip Fanwick for his kind help in obtaining statistical information from the Cambridge Structural Database, Prof. Debbie Crans for stimulating discussions, and Prof. Jeff Bolin for helpful advice on structure refinement.

REFERENCES

Allen, F. H., & Kennard, O. (1993) *Chem. Des. Autom. News 8*, 31−37.
Barbera, A., Rodríguez-Gil, J. E., & Guinovart, J. J. (1994) *J. Biol. Chem. 269*, 20047−20053.
Barford, D., Flint, A. J., & Tonks, N. K. (1994) *Science 263*, 1397−1403.
Blenis, J. (1993) *Proc. Natl. Acad. Sci. U.S.A. 90*, 5889−5892.
Borah, B., Chen, C. W., Egan, W., Miller, M., Wlodawer, A., & Cohen, J. S. (1985) *Biochemistry 24*, 2058−2067.
Charbonneau, H., & Tonks, N. K. (1992) *Annu. Rev. Cell Biol. 8*, 463−493.
Cornman, C. R., Geiser-Bush, K. M., & Singh, P. (1994) *Inorg. Chem. 33*, 4621−4622.
Crans, D. C., & Simone, C. M. (1991) *Biochemistry 30*, 6734−6741.
Crans, D. C., & Shin, P. K. (1994) *J. Am. Chem. Soc. 116*, 1305−1315.
Crans, D. C., Chen, H., Anderson, O. P., & Miller, M. M. (1993) *J. Am. Chem. Soc. 115*, 6769−6776.
Davis, J. P., Zhou, M.-M., & Van Etten, R. L. (1994a) *Biochemistry 33*, 1278−1286.
Davis, J. P., Zhou, M.-M., & Van Etten, R. L. (1994b) *J. Biol. Chem. 269*, 8734−8740.
DeMaster, E. G., & Mitchell, R. E. (1973) *Biochemistry 12*, 3616−3621.
Denu, J. M., Lohse, D. L., Vijayalakshmi, J., Saper, M. A., & Dixon, J. E. (1996) *Proc. Natl. Acad. Sci. U.S.A. 93*, 2493−2498.
Egloff, M.-P., Cohen, P. T. W., Reinemer, P., & Barford, D. (1995) *J. Mol. Biol. 254*, 942−959.
Evans, B., Tishmack, P. A., Pokalsky, C., Zhang, M., & Van Etten, R. L. (1996) *Biochemistry 35*, 13609−13617.
Jones, T. A., Zou, J. Y., Cowan, S. W., & Kjeldgaard, M. (1991) *Acta Crystallogr. A47*, 110−119.
Kostrewa, D., Choe, H. W., Heinemann, U., & Saenger, W. (1989) *Biochemistry 28*, 7592−7600.
Kraulis, P. J. (1991) *J. Appl. Crystallogr. 24*, 946−950.
Lerea, K. M., Tonks, N. K., Krebs, E. G., Fischer, E. H., & Glomset, J. A. (1989) *Biochemistry 28*, 9286−9292.
Lindquist, R. N., Lynn, J. L., Jr., & Lienhard, G. E. (1973) *J. Am. Chem. Soc. 95*, 8762−8768.
Lindqvist, Y., Schneider, G., & Vihko, P. (1994) *Eur. J. Biochem. 221*, 139−142.
Logan, T., Zhou, M.-M., Nettesheim, D. G., Meadows, R. P., Van Etten, R. L., & Fesik, S. W. (1994) *Biochemistry 33*, 11087−11086.
Macara, I. G. (1980) *Trends Biochem. Sci. 5*, 92−94.
Messerschmidt, A., & Wever, R. (1996) *Proc. Natl. Acad. Sci. U.S.A. 93*, 392−396.
Modarress, K. J., Cavanaugh, A. H., Chakraborti, P. K., & Simons, S. S., Jr. (1994) *J. Biol. Chem. 269*, 25621−25628.
Murmann, R. K. (1977) *Inorg. Chem. 16*, 46−51.
Nielson, F. H. (1995) *Metal Ions Biol. Syst. 31*, 543−573.
Otwinowski, A. (1993) DENZO, *Data Collection and Processing* (Sawyer, L., Isaacs, N., & Bailey, S., Eds.) pp 56−62, SERC Daresbury Laboratory, Warrington, U.K.
Pope M. T., & Dale, B. W. (1968) *Q. Rev. Chem. Soc. 22*, 527−548.
Ramachandran, G. N., & Sasisekharan, V. (1968) *Adv. Protein Chem. 23*, 283−437.

Ray, W. J., Jr., Burgner, J. W., II, & Post, C. B. (1990) *Biochemistry 29*, 2770−2778.
Ray, W. J., Jr., Burgner, J. W., II, Deng, H., & Callender, R. (1993) *Biochemistry 32*, 12977−12983.
Saini, M. S., Buchwald, S. C., Van Etten, R. L., & Knowles, J. R. (1981) *J. Biol. Chem. 256*, 10453−10455.
Smith, C. A., & Rayment, I. (1996) *Biochemistry 35*, 5404−5417.
Smith, T. J. (1995) *J. Mol. Graphics 13*, 122−125.
Stuckey, J. A., Schubert, H. L., Fauman, E. B., Zhang, Z.-Y., Dixon, J. E., & Saper, M. A. (1994) *Nature 370*, 571−574.
Su, X.-D., Taddei, N., Stefani, M., Ramponi, G., & Nordlund, P. (1994) *Nature 370*, 575−578.
Tracey, A. S., Li, H., & Gresser, M. J. (1990) *Inorg. Chem. 29*, 2267−2271.
Tronrud, D. G., Ten Eyck, L. F., & Matthews, B. W. (1987) *Acta Crystallogr. A43*, 489−501.
Van Etten, R. L., Waymack, P. P., & Rehkop, D. M. (1974) *J. Am. Chem. Soc. 96*, 6782−6785.
Veenstra, T. D., & Lee, L. (1994) *Biophys. J. 67*, 331−335.
Waheed, A., Laidler, P. M., Wo, Y.-Y. P., & Van Etten, R. L. (1988) *Biochemistry 27*, 4265−4273.
Wlodawer, A., Miller, M., & Sjolin, L. (1983) *Proc. Natl. Acad. Sci. U.S.A. 80*, 3628−3631.
Wo, Y.-Y. P., Zhou, M.-M., Stevis, P., Davis, J. P., Zhang, Z.-Y., & Van Etten, R. L. (1992) *Biochemistry 31*, 1712−1721.
Zhang, M., Van Etten, R. L., & Stauffacher, C. V. (1994a) *Biochemistry 33*, 11097−11105.
Zhang, M., Van Etten, R. L., Lawrence, C. M., & Stauffacher, C. V. (1994b) *J. Mol. Biol. 238*, 281−283.
Zhang, M., Stauffacher, C. V., & Van Etten, R. L. (1995) *Adv. Protein Phosphatases 9*, 1−23.
Zhang, Z., Harms, E., & Van Etten, R. L. (1994) *J. Biol. Chem. 269*, 25947−25950.
Zhang, Z.-Y., & Van Etten, R. L. (1991) *Biochemistry 30*, 8954−8959.
Zhang, Z.-Y., & Dixon, J. (1994) *Adv. Enzymol. 68*, 1−36.
Zhou, M.-M., Davis, J. P., & Van Etten, R. L. (1993) *Biochemistry 32*, 8479−8486.

BI961804N